Annual Report of Iwate Medical University
Center for Liberal Arts and Sciences
No. 54(2019), 1–8.

Near-infrared-ray computed tomography with 850-nm peak and high spatial resolutions

Eiichi SATO[a], Akiko YOSHIDA[b], Toshihiro SOMEYA[c], Daiki YOSHIZAWA[a],
Mana MORIMOTO[a], Toshiaki MINE[a], Yasuyuki ODA[a],
Sohei YOSHIDA[d], Kunihiro YOSHIOKA[d], Yuichi SATO[e]

[a] Department of Physics, Iwate Medical University, 1-1-1 Idaidori, Yahaba, Iwate 028-3694, Japan
[b] Department of Clinical Genetics, School of Medicine, Iwate Medical University, 2-1-1 Idaidori, Yahaba, Iwate 028-3695, Japan
[c] Department of Central Clinical Laboratory, Iwate Medical University Hospital, 2-1-1 Idaidori, Yahaba, Iwate 028-3695, Japan
[d] Department of Radiology, School of Medicine, Iwate Medical University, 2-1-1 Idaidori, Yahaba, Iwate 028-3695, Japan
[e] Central Radiation Department, Iwate Medical University Hospital, 2-1-1 Idaidori, Yahaba, Iwate 028-3695, Japan

(Accepted December 6, 2019)

Abstract

To improve the spatial resolution in near-infrared-ray computed tomography (NIR-CT), a first-generation scanner was constructed in the first living-body window. The NIR photons are produced from an 850-nm-peak light-emitting diode, and penetrating photons from an object are selected using an infrared filter and detected using a phototransistor (PT). To improve the spatial resolution, we used two sets of polyacetal collimators of 1.0-mm diameter and 5.0-mm length and Cu pinholes of 1.0-mm diameter. The NIR line beam is roughly formed using the first collimator, and the beam diameter is reduced using the first Cu pinhole. The second pinhole is set behind the object to detect the penetrating photons. The second collimator is attached to the PT to improve the spatial resolution. The NIR-CT is realized by repeated translations and rotations of the object, which were performed in steps of 0.25 mm and 1.0°, respectively. The spatial resolutions were determined as 1.0 × 1.0 mm^2. The scanning time and total rotation angle for the CT were 9.8 min and 180°, respectively.

Keywords: NIR-CT, 850-nm LED, living-body window, penetrating photon detection, high-sensitivity imaging, high spatial resolution

1. Introduction

Near infrared-ray (NIR) photons in the living-body window are useful for penetrating biomedical objects, and several NIR computed tomography (CT) scanners [1, 2] have been developed. To avoid X-ray exposure, we have constructed a first-generation 940-nm NIR-CT scanner [3] for performing physical experiments in our medical university. Parallelly, we have been improving the first-generation photon-counting energy-dispersive X-ray CT scanner [4, 5] using a cadmium telluride detector, and the spatial resolutions have been improved to approximately 0.3×0.3 mm^2.

Although the NIR camera can be used to perform NIR-CT, it is difficult to improve the spatial resolution with current technologies. The NIR photons penetrate the object and are reflected, diffracted, and scattered by the object. Therefore, it is important to detect only the penetrating photons from the object to improve the spatial resolution and to obtain the penetrating image such as an X-ray tomogram.

It is known that the wavelength range of 700–900 nm is called the first living-body window [6], and the photons in the window can penetrate water and hemoglobin. Therefore, we also performed NIR-CT [7] using an 850-nm-peak light-emitting diode (LED) and a 900-nm-peak sensitivity phototransistor (PT). In this CT, we used a graphite collimator of 1.5-mm diameter and 15-mm length for the PT to detect the penetrating photons. With this NIR-CT, a sufficient NIR intensity was obtained on using the LED and PT. However, the spatial resolutions were approximately 2×2 mm^2, and it was difficult to improve the resolution.

In the case wherein a sufficient NIR intensity for the CT is obtained on using a small-diameter line beam, image processing that is equivalent to high-sensitivity imaging can be performed using a computer program, as the NIR intensity substantially decreases as the living-tissue thickness increases even when the living body-window photons are used.

The major objectives of our research are as follows: to reduce the line-beam diameter and the scattering-diffracting photon count, to increase the detecting sensitivity using a PT, to perform image processing that is equivalent to high-sensitivity CT, and to simultaneously obtain two different-sensitivity tomograms. Therefore, we constructed an 850-nm-peak NIR-CT scanner in the first living-body window and performed dual-sensitivity CT.

2. Experimental methods

2.1. NIR-CT scanner

The main components of the NIR-CT scanner are presented in Fig. 1. An object was exposed to the NIR photons from the LED device, and the PT device detects the penetrating photons. We fixed the LED and PT devices and the object on a turntable (Siguma Koki, SGSP-60YAW-OB) that oscillates on a translation stage (Siguma Koki, SGSP-26-100). The translation stage and the turntable are driven by a two-stage controller (Siguma Koki, SHOT-602). The PT-device output is input to an analog-to-digital converter (ADC; Contec, AI-1608AY-USB), and the ADC output is sent to a personal computer (PC). Thus, translation is achieved by the object oscillation, and the object on the turntable rotates by 1.0° between translations. The velocity and stroke of the translation were 25 mm/s and 60 mm, respectively.

Figure 2 shows the experimental setup around the object. The LED-to-PT distance is 170 mm, and the turntable-center-to-PT distance is 50 mm. In the scanner, we used two sets of polyacetal collimators of 1.0-mm diameter and 5.0-mm length and Cu pinholes of 1.0-mm diameter; the pinhole is fabricated using an electric substrate (Sunhayato, NZ-E40K). The NIR line beam is roughly formed using the first collimator, and the

beam diameter is reduced using the first pinhole in front of the object. Subsequently, the refracted and scattered photon counts are reduced using the second pinhole, and the spatial resolution is determined by the second collimator attached to the PT. The visible-ray photons are shaded by the IR filter (Fujifilm, IR-80) attached to the collimator, and almost only the penetrating NIR photons can be detected. While performing the tomography, the reciprocating translation and rotation are repeated.

To reconstruct the tomograms, the convolution back-projection method is used, and the translation and rotation are performed in steps of 0.25 mm and 1.0°, respectively. The scanning time is proportional to the total rotation angle of 180° and is 9.8 min.

Figure 3 shows the electric circuits of the LED (OptoSupply, OSI53CA3131A) and PT (New Japan Radio, NJL7112B) devices. The LED forward current of 0.10 A is regulated using a 1.0-kΩ variable resistor [Fig. 3(a)]. The visible-ray photons are absorbed by the IR filter, and only NIR photons are detected. The PT output is produced by the emitter-follower circuit, and the minimum PT output is determined by a 0.51-MΩ fixed resistor. Next, the PT output is regulated to 4.98 V using a 1.0-MΩ variable resistor [Fig. 3(b)].

In this experiment, high-sensitivity imaging was performed using a computer program. The output voltages of 4.98 and 0 V from the PT device correspond to the ADC-digital outputs of 49,086 and 32,768, respectively. Thus, high-sensitivity imaging with an amplification gain of α can be performed by decreasing the maximum digital output of the air D, which is given by

$$D = 32{,}768 + (49{,}086 - 32{,}768) / \alpha. \qquad (1)$$

At an α value of 30, the calculated value of D is 33,312.

2.2. NIR-spectra measurement

To measure the NIR spectra, we used a spectrometer (Hamamatsu Photonics, C10083CA) and a light fiber of 1.5-m length. The wavelength calibration was performed using a readily available laser module (CivilLaser, 850 nm, 30 mW).

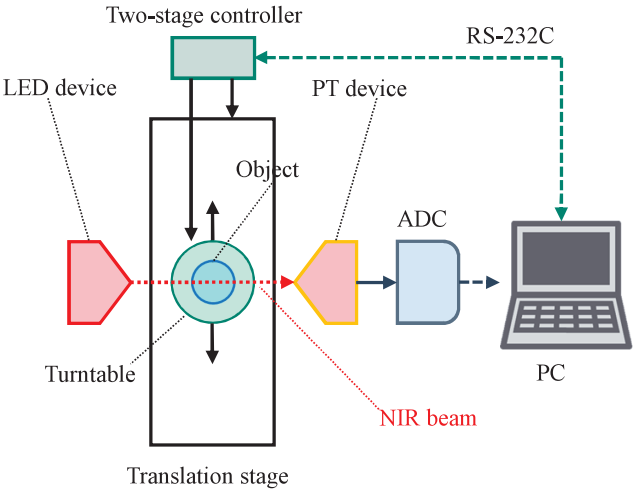

Fig. 1 Main components of the NIR-CT scanner. The NIR photons from the LED device are detected using the PT device, and the PT device output is input to the PC through an ADC. The translation stage and the turntable are driven by the two-stage controller.

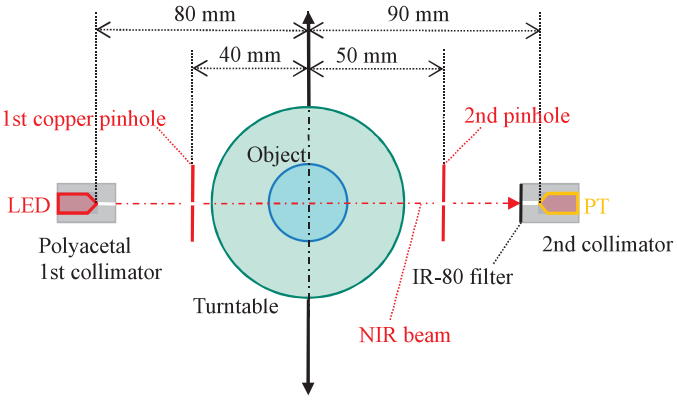

Fig. 2 Experimental arrangement of the NIR-CT scanner around the object. The LED and PT devices are fixed, and the translation is accomplished by the turntable oscillations on the translation stage; the object is placed on the turntable. The line beam is formed using a set of collimator and pinhole in front of the object. The scattering-diffracting photon count is reduced using a pinhole behind the object, and the spatial resolution is determined by a collimator attached to the detector.

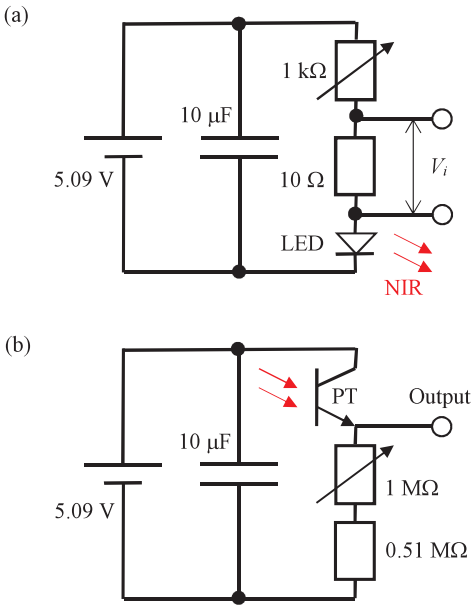

Fig. 3 Circuit diagram of the LED and PT devices. (a) The LED-forward current is measured using the 10-Ω resistor and regulated by the 1-kΩ variable resistor. (b) In the PT device, the output voltage is maximized to 4.98 V using a 1-MΩ variable resistor at an α of 1.

3. Results

3.1. NIR spectra

Figure 4 shows the NIR spectra, and the peak wavelength measured was 850 nm. Using the IR-80 filter, few of the low-wavelength photons were absorbed, and the peak wavelength varied slightly.

3.2. Tomography

Tomography was accomplished at a relative amplifier gain α of 1 and 30. The tomograms are obtained as JPEG files, and the maximum and minimum gray-value densities are defined as white and black, respectively.

The NIR tomography of two iron rods of diameters 0.5 and 1.0 mm is presented in Fig. 5. The two rods were visible at an α of 1. When α was increased to 30, the 0.5-mm-diameter rod could not be observed, and the diameter of the image of the 1.0-mm-diameter rod decreased.

Figure 6 shows the tomography of two glass vials of 15-mm diameter filled with indigo-carmine solutions of 10 and 20 mg/ml, respectively. At an α of 1, the NIR photons easily penetrated the vial filled with the 10-mg/ml solution. However, the NIR photons did not penetrate the 20-mg/ml solution. The vial-image diameters decreased slightly as α increased.

Figure 7 shows the tomography of a shrimp head. At an α of 1, the head and legs were observed at a high contrast. As α increased, both the head and leg dimensions decreased slightly.

The tomography of the bone and muscle of a chicken-wing tip is shown in Fig. 8. At an α of 1, the outlines of the bone and muscle were observed. On increasing α to 30, the image dimensions of both the bone and muscle decreased slightly. However, the bone in the muscle was not observed.

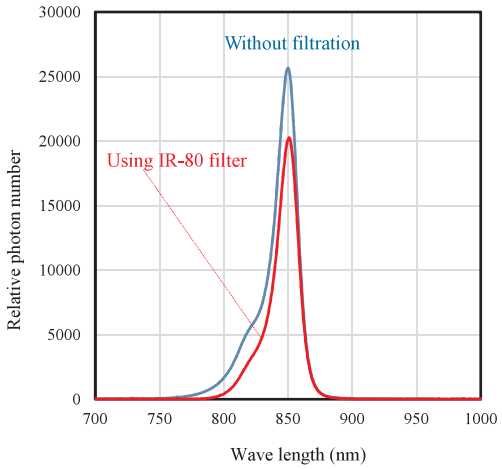

Fig. 4 NIR spectra after the wavelength calibration. Few short-wavelength NIR photons were absorbed by the IR filter.

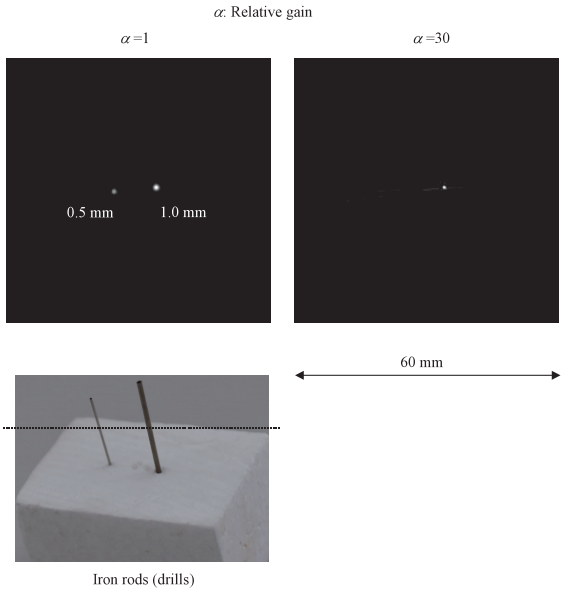

Fig. 5 Tomography of the two iron rods for roughly determining the spatial resolution. In both gains, the 1.0-mm-diam rod could be observed.

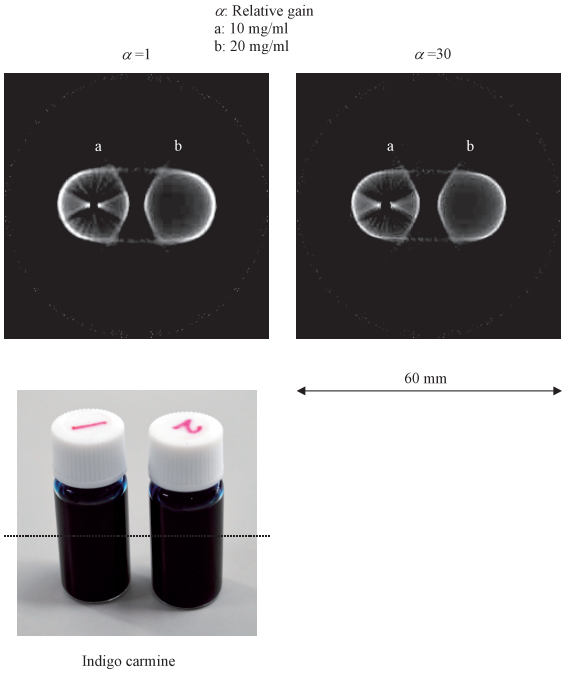

Fig. 6 Tomography of two glass vials filled with indigo-carmine solutions of two different densities of 10 and 20 mg/ml. The NIR photons easily penetrated the 10-mg/ml solution at a low incident angle. The image diameters of the two vials slightly decreased with increasing α.

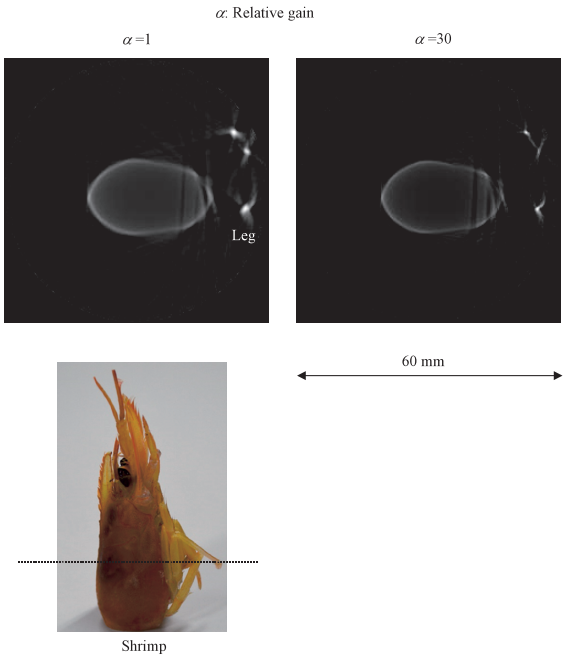

Fig. 7 Tomography of a shrimp head. The outlines of the head and legs were visible at an α of 1. The image dimensions of the head and legs decreased slightly at an α of 30.

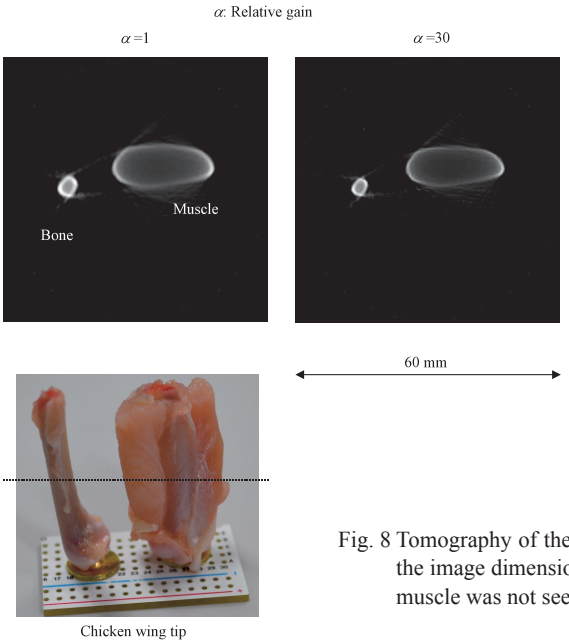

Fig. 8 Tomography of the bone and the muscle of chicken-wing tip. With increasing gain α, the image dimensions of both the bone and muscle decreased slightly. The bone in the muscle was not seen at an α of 30.

4. Discussion

NIR-CT was performed using LED and PT devices in the first living-body window (Table 1). The peak wavelength of the LED was determined as 850 nm on using a spectrometer and a laser module for the wavelength calibration. Next, the PT high-sensitivity wavelength is 900 nm in the data table, and it was easy to detect NIR penetrating photons from the LED using the IR filter. In the laboratory, NIR photons are produced from a fluorescent lamp, and a dark room with blue-LED lighting might be useful for performing high-sensitivity imaging at an α beyond 50.

The 850-nm-peak NIR photons easily penetrated a glass vial filled with 10-mg/ml indigo-carmine at low incident angles, and the photons reflected around the vial at large incident angles. As the photons are also refracted and scattered, the penetrating photons should be detected by a set of a pinhole and collimator placed behind the object.

To detect the NIR photons, we used the PT in conjunction with an emitter-follower circuit. In the circuit, the detection sensitivity is proportional to the emitter-to-ground resistance. The maximum resistance of the PT device was approximately 1.51 MΩ, and the resistance can easily be increased to 100 MΩ.

The measured effective penetration depth increases on increasing the detection sensitivity and the NIR-luminous intensity. Therefore, the detection sensitivity can easily be increased, and the intensity (brightness) substantially increases on using the laser module.

The NIR intensity obtained on using the LED decreases as the LED-to-PT distance increases, and this distance should thus be minimized. We have constructed an NIR-CT scanner using the 850-nm laser module described above, and sufficient NIR intensities can be obtained even when a large source-to-PT distance is used.

The pixel dimensions of the reconstructed CT image were 0.25×0.25 mm^2 corresponding to the scan step. However, the original spatial resolution was primarily determined by the collimator diameter of 1.0 mm for the PT. As the amplifier gain increased, although we observed an iron rod of 1.0-mm diameter, an iron rod 0.5-mm diameter could not be observed easily. Thus, the spatial resolutions were roughly estimated to be 1×1 mm^2.

Table 1 NIR-CT specifications. Compared with former experiment, the spatial resolutions were improved from 2.0×2.0 to 1.0×1.0 mm^2 using a collimator and two pinholes at a scan step of 0.25 mm.

Specifications	
Generation type	1st
Beam type	Line
Beam diameter (mm)	Approx.1
Source	850-nm-NIR LED
Detector	VR PT+IR-80 filter
Peak wavelength (nm)	850
Stroke (mm)	60
Turntable diameter (mm)	60
Collimator diameter for detector (mm)	1.0
Pinhole diameter (mm)	1.0
Translation velocity (mm/s)	25
Translation step (mm)	0.25
Rotation step (º)	1.0
Total rotation angle (º)	180
Scanning time (min)	9.8
Reconstructed pixel dimensions (mm^2)	0.25×0.25
Spatial resolution (mm^2)	Approx. 1×1

5. Conclusions

We constructed an 850-nm NIR-CT scanner to improve the spatial resolution in the detection of photons penetrating an object. The scanning time was 9.8 min for a translation step of 0.25 mm, a rotation step of 1.0°, and a total rotation angle of 180°. It is difficult to obtain a sufficient penetrating NIR intensity using an LED and a collimator of a small diameter of less than 1 mm for the PT. Therefore, an 850-nm laser module should be used to improve the spatial resolution in future research.

Acknowledgments

This work was supported by Grants from Keiryo Research Foundation, Promotion and Mutual Aid Corporation for Private Schools of Japan, Japan Science and Technology Agency (JST), and JSPS KAKENHI (17K10371, 17K09068, 17K01424, and 17H00607). This was also supported by a Grant-in-Aid for Strategic Medical Science Research (S1491001 and 2014–2018) from the Ministry of Education, Culture, Sports, Science and Technology of Japan.

References

[1] Dehghani, H., Pogue, B.W., Poplack, S.P., Paulsen, K.D., "Multiwavelength three-dimensional near-infrared tomography of the breast: initial simulation, phantom, and clinical results," Appl. Opt. 42, 135-145 (2003).

[2] Osawa, S., Murata, T., Hashimoto, F., Teramoto, A., Fujita, H., "Basic study on the near-infrared light computed tomography: development of the experimental systems using a digital single-lens reflex camera," Med. Imag. Inf. Sci. 32, 44-47 (2015).

[3] Sato, E., Oda, Y., Yuichi, S., Yamaguchi, S., Ishii, T., Hagiwara, O., Matsukiyo, H., Watanabe, M., Kusachi, S.,

"Investigation of a near-infrared-ray computed tomography scanner," Proc. SPIE 9969, 99690I-1-6 (2016).

[4] Sato, E., Kosuge, Y., Yamanome, H., Mikata, A., Miura, T., Oda, Y., Ishii, T., Hagiwara, O., Matsukiyo, H., Watanabe, M., Kusachi, S., "Investigation of dual-energy X-ray photon counting using a cadmium telluride detector with dual-energy selection electronics," Rad. Phys. Chem. 130, 385-390 (2017).

[5] Matsukiyo, H., Sato, E., Oda, Y., Ishii, T., Yamaguchi, S., Sato, Y, Hagiwara, O., Enomoto, T., Watanabe, M., Kusachi, S., "Investigation of quad-energy photon counting for X-ray computed tomography using a cadmium telluride detector," Appl. Radiat. Isot. 130, 54-59 (2017).

[6] Shimadzu; 2018. http://www.med.shimadzu.co.jp/products/om/qa01.html#02. Accessed 18 Dec. 2018.

[7] Sato, Y., Takaoka, A., Sato, T., Sato, E., Oda, Y., Yoshida, S., Moriyama, H., Hagiwara, O., Matsukiyo, H., Enomoto, T., Watanabe, M., Kusachi, S., "850-nm-peak high-sensitivity near-infrared-ray computed tomography scanner in the living-body window," Health. Technol. 8, 205-210 (2018).